Effect of sintering temperature on the structural and physical properties of forsterite using amorphous rice husk silica as refractory precursors

Simon Sembiring, Agus Riyanto, Leny Rumiyanti, Zipora Sembiring & Rudy Situmeang

Journal of the Australian Ceramic Society

ISSN 2510-1560
Volume 56
Number 2

J Aust Ceram Soc (2020) 56:433-440
DOI 10.1007/s41779-019-00346-2

Springer

Journal of the Australian Ceramic Society (2020) 56:433–440
https://doi.org/10.1007/s41779-019-00346-2

RESEARCH

Effect of sintering temperature on the structural and physical properties of forsterite using amorphous rice husk silica as refractory precursors

Simon Sembiring[1] · Agus Riyanto[1] · Leny Rumiyanti[1] · Zipora Sembiring[2] · Rudy Situmeang[2]

Received: 18 July 2018 / Revised: 3 February 2019 / Accepted: 19 March 2019 / Published online: 17 April 2019

Abstract
This study aims to investigate the effect of sintering temperatures on both the phase formation and physical characteristics of forsterite prepared from rice husk silica and magnesium nitrate hydrate. The samples were subjected to sintering temperatures of 1000–1300 °C, and the development of structures was characterized using Fourier transform infrared (FTIR) spectroscopy, X-ray diffraction (XRD), and scanning electron microscopy (SEM). Some physical properties include density, porosity, hardness, bending strength, and thermal expansion coefficient of the samples were measured. It is concluded that forsterite formation started at 1000 °C, and its abundance increased slowly from an increased temperature up to 1300 °C, resulting in increased phase contents from 87.7 to 90.0 wt%. Thermal expansion coefficient of the samples with increasing temperature of sintering from 1100 to 1300 °C reaches the relatively constant value of 9.1×10^{-6}/°C, with the main crystalline phase being forsterite.

Keywords Refractory · Rice husk · Sintering · Forsterite · Structure

Introduction

Forsterite (Mg_2SiO_4) is the magnesium-rich end-member of the olivine solid solution series [1], and it is endowed with the low dielectric constant as well as low thermal expansion coefficient, which makes as an excellent insulator, high-thermal resistant material, refractoriness, and good biocompatibility. In the previous study [2], it was reported that thermal expansion of forsterite is 9.2×10^{-6}/°C. Another interesting property of forsterite which makes this material great importance as refractory material is its very high melting temperature (1890 °C) [3], low thermal expansion and excellent insulation properties even at high temperatures [4], and also suitable for the use of thermal insulation. In addition, forsterite exhibits good chemical stability and low electrical conductivity [5].

Forsterite has been synthesized by various techniques, including the conventional solid-state reaction to periclase (MgO) and silica (SiO_2) [6], the mechanical activation of a talc and magnesium carbonate powder mixture [7], the polymer precursor method [8], and the sol–gel method [9]. The production of forsterite through the solid-state reaction usually requires high temperature and long reaction time, while the sol–gel process can promote molecule-level of mixing, results in high degree of homogeneity, which leads to reduced temperature and prevention of phase segregation during heating. In the previous study [10], it was found that nano-crystalline forsterite with the particle size of 17–20 nm could be produced using sol–gel method followed by sintering at 800 °C, because the initial formation of forsterite occurred at 760 °C and a complete formation of crystalline forsterite at 800 °C [3]. Also, many efforts have been made to improve the workability of forsterite, including reduction of the firing temperature by the addition of alumina [11] or low melting point glasses [12]. Another possible way to produce forsterite materials at lower temperatures is through the glass–ceramic process. Indeed,

✉ Simon Sembiring
simonsembiring2@gmail.com

[1] Department of Physics, Faculty of Mathematics and Natural Sciences, Universitas Lampung, Bandar Lampung, Lampung 35145, Indonesia

[2] Department of Chemistry, Faculty of Mathematics and Natural Sciences, Universitas Lampung, Bandar Lampung, Lampung 35145, Indonesia

several investigations report the devitrification of forsterite as a secondary crystalline phase in glass–ceramics belonging to different composition systems [13–17].

In general, the refractory material should exhibit high thermal shock resistance, high fracture toughness, and low thermal expansion. For these reasons, thermal resistance parameters and thermal shock behaviors of refractory forsterite have been the subject of extensive studies. Considerable effort has also been devoted to synthesize forsterite material for biomedical application [18] and found very high fracture toughness and hardness at sintering temperature of 1400 °C. Ni et.al. [9] have successfully prepared forsterite with high purity and homogeneity after the sample was sintered in the temperature range of 1000 to 1500 °C, while Lee et. al. [19] found that pure forsterite could be obtained after sintering the powder mixture of 1300 °C. It is, however, very difficult to avoid the secondary phase formation such the polymorphs of silica, periclase, and enstatite.

In the context of ceramic material, rice husk ash as agriculture waste is known to contain silica inconsiderable amount, which could be extracted by a relatively simple method to obtain high purity and active silica. Several types of researches [20–22] reported that pure silica can be extracted from the purity in the range of 94–98% as amorphous. Several studies have been also conducted to utilize rice husk silica to produce various silica-based materials, such as production of nano-silica [23, 24], zeolites [25], silica aerogel [26], glass–ceramic materials in the SiO_2–Na_2O–CaO [27], SiO_2/C composite [28], forsterite–nepheline glass–ceramic [29], cement paste and concrete [30], cordierite [31], and forsterite [32].

This current study aimed to quantify the phase composition and explored the relationship between composition and physical characteristics of refractory forsterite. The present study is concerned on the effect of different sintering temperatures on the phase composition and physical characteristics of refractory forsterite prepared from amorphous rice husk silica. To gain insight on several basic characteristics, the phase composition of refractory forsterite with different sintering temperatures was studied by means of FTIR, XRD, and SEM studies.

Experimental methods

Materials and instruments

Silica from rice husk and magnesium nitrate $(Mg(NO_3)_2 \cdot 6H_2O$ (Merck, kGaA, Damstadt, Germany) were used as raw materials. KOH 5%, NaOH 5%, and HCl 10% used are reagent grade obtained from Merck. The equipment used are a PerkinElmer FTIR Spectrometer, an automated Shimadzu XD-610 X-ray diffractometer, a Philips-XL SEM, Nabertherm electrical furnace, magnetic stirrer, and a microbalance Mettler Instrument AG, CH-8806 Greifensee-Zurich.

Procedure

Synthesis of forsterite using sol gel method was performed in two steps: (i) preparation of silica and magnesium sol from rice husk and magnesium nitrate hydrate, respectively and (ii) preparation of forsterite powder.

Preparation of silica and magnesium sol

Preparation of silica sol was conducted following the procedures that have previously been applied [33]. The dried husk (50 g) was stirred in 500 mL of 5% KOH solution. The mixture was boiled in a baker glass for 30 min and allowed to cool to room temperature and left for 24 h. The mixture was filtered to separate the filtrate which contains silica (silica sol). Magnesium sol was prepared by dissolving 30 g of $(Mg(NO_3)_2 \cdot 6H_2O$ into 100 mL ethanol in a beaker glass under magnetic stirring for 4 h.

Preparation of forsterite powder

Preparation of the solid forsterite was treated following the procedures that previously been used [33]; calculated quantities of silica sol were added under stirring to the appropriate volume of magnesium sol to give the ratios of magnesium oxide and silica ($MgO:SiO_2$) as a mass ratio of 3:2. The mixture was heated at 90 °C under continuous stirring to transform the sample (sol) into gel. The gel was aged for 3 days, rinsed repeatedly with deionized water to remove the excess of acid and alkali and then oven dried at 110 °C for 6 h and grounded into powder with the size of 150 meshes. The powder was pressed in a metal die with the pressure of with the pressure of 2×10^4 N/m^2 to produce cylindrical pellet, and then the pellet was sintered at 1000, 1100, 1200, and 1300 °C, using temperature programmed with a heating rate of 3 °C/min and holding time of 4 h at peak temperatures.

Characterization

A PerkinElmer FTIR was used for the investigation of functional groups of the forsterite. The X-ray diffraction data were collected using an automated Shimadzu XD-610 X-ray diffractometer equipped with a scintillation counter. The operating conditions used were Cu Kα radiation ($\lambda = 0.15418$ Å), produced at 40 kV and 30 mA, with a 0.15° receiving slit and 2θ ranges from 5 to 100° with a step size of 0.02. Microstructural analysis was conducted with scanning electron microscopy (SEM) Philips-XL on thermally etched samples. Archimedes method using distilled water as liquid media was used to measure bulk density and apparent porosity [34].

A Zwick tester was used to measure the Vickers hardness, with three replicate measurements for each loading position. Bending strength or Modulus Rupture (MOR) was determined by the three-point method following the ASTM C268-70. The measuring of thermal expansion coefficient was conducted using dilatometry (Harrop Dilatometer) in the temperature range of 150–600 °C at a heating rate of 5 °C/min. The linear thermal expansion coefficient (α) was automatically calculated using the general equation: $\alpha = (\Delta L/L)(1/\Delta T)$. ΔL is the increase in length, ΔT is the temperature interval over which the sample is heated, and L is the original length of the specimen.

Results and discussion

Characteristics of synthesized refractory forsterite precursors

Figure 1(a) shows the infrared spectrum of the unsintered sample, and Fig. 1(b–e) reveals the spectra of the samples sintered at different temperatures. For the unsintered sample (Fig. 1(a)), the most obvious peak is located at 3436 cm^{-1}, which is commonly attributed to the stretching vibration of O–H bonds present in $Mg(OH)_2$, $Si(OH)_4$, and trapped water molecules. The contribution of water is confirmed by the absorption band at 1562 cm^{-1}, which is commonly assigned to the bending vibration of H-OH bonds [35]. Another small band observes dislocated at 1340 cm^{-1}, which is the characteristic stretching vibration of the entrapped nitrate ions of $Mg(NO_3)_2{\cdot}6H_2O$. The wide and weak peak located at 1083 cm^{-1} is commonly assigned to the stretching vibration of Si–O–Si. The presence of absorption peaks at 1562 and 1083 cm^{-1} suggest that the sample is still dominated by $Si(OH)_4$. Figure 1(b–e) indicates the significant effect of thermal treatment on the functionality of the samples. The most obvious change is the absence of peaks associated with nitrate ions, confirming the release of the nitrogenous gases during the heating process. In addition, the intensity of the band assigned to O–H bonds decreased due to the evaporation of water and the release of OH species through the decomposition of $Si(OH)_4$ and $Mg(OH)_3$ molecules into oxides. As a consequence, the intensity of the absorption band at ~ 473 cm^{-1}, assigned to Si–O–Si vibration, increased and accompanied by the emergence of a new band at ~ 559 cm^{-1} assigned to Mg–O. The increased intensity of Si–O–Si indicates that the $Si(OH)_4$ has been converted to SiO_2, which is in agreement with the decreased intensity of the peaks assigned to O–H bonds, while the emergence of the peak attributed to Mg–O is an indication of the conversion of $Mg(OH)_3$ into magnesium oxides. Another important finding is the formation of forsterite at 1100 °C, which continues to develop at higher temperatures, as indicated by the emergence of the absorption band at 993 cm^{-1}, which is assigned to Si–O–Mg linkages, and the band at 917 cm^{-1} which implies the existence of an $MgO\text{-}SiO_2$ structure [36]. In the all spectra of the samples, a small peak was observed at ~ 2328 cm^{-1}, which is commonly assigned to the vibration band of C–O [35] probably originated from atmospheric CO_2 absorbed by the sample during its preparation.

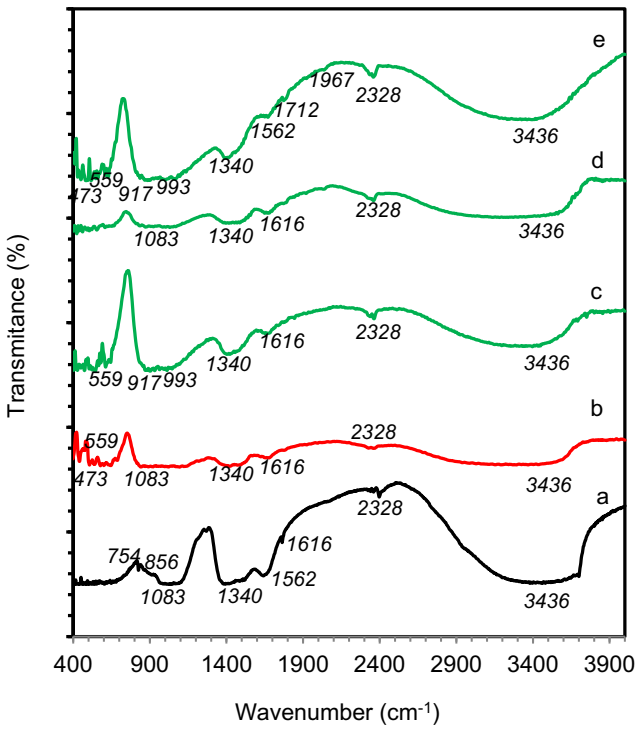

Fig. 1 FTIR spectra of non-sintered sample (a) and the samples sintered at different temperatures (b) 1000 °C, (c) 1100 °C, (d) 1200 °C, and (e) 1300 °C, with ratio of MgO to SiO_2 is 3:2

The XRD patterns of the unsintered and sintered samples at 1000, 1100, 1200, and 1300 °C were recorded, and the crystalline phases formed are shown in Fig. 2(a–e). The phases identified with the PDF diffraction lines [37]; the results show the presence of forsterite 36.7° (PDF-34-0189), cristobalite 21.98° (PDF-34-1425), MgO/periclase 42.9° (PDF45-0946), and enstatite/$MgSiO_3$ 28.2° (PDF-11-0273).

For the unsintered sample (Fig. 2(a)) the presence of enstatite was clearly detected. This suggests that at this condition the formation of enstatite has commenced. Increasing the sintering temperatures was found to lead to substantial differences between the samples. The sample sintered at a temperature of 1000 °C (Fig. 2(b)) is marked by undetected the intensity of enstatite, while the intensities of forsterite, cristobalite, and periclase increased quite significantly compared to that observed in the unsintered sample (Fig. 2(a)). The temperature of forsterite formation observed in this study is lower than those reported by others using TEOS [38], in which it was reported forsterite formation started at 1000 °C and the formation of forsterite was evident at 1100 °C. Such an

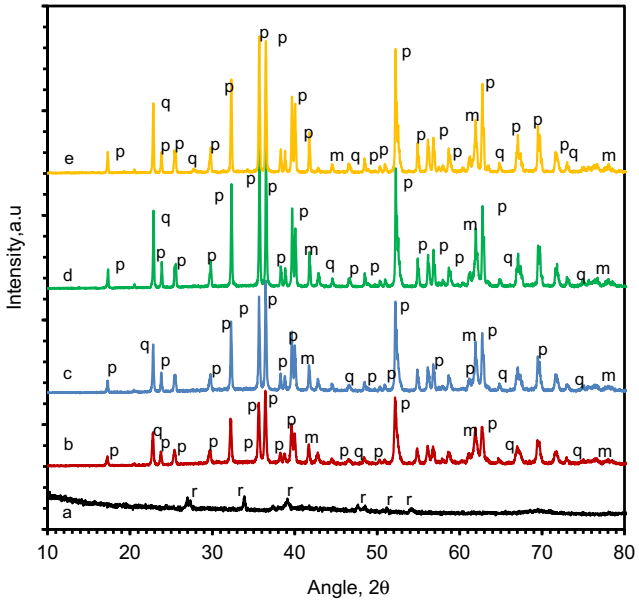

Fig. 2 X-ray diffraction patterns of non-sintered sample (a) and the samples sintered at different temperatures (b) 1000 °C, (c) 1100 °C, (d) 1200 °C, and (e) 1300 °C, using Cu Kα radiation. Legend: p forsterite, q cristobalite, r enstatite ($MgSiO_3$), m periclase (MgO)

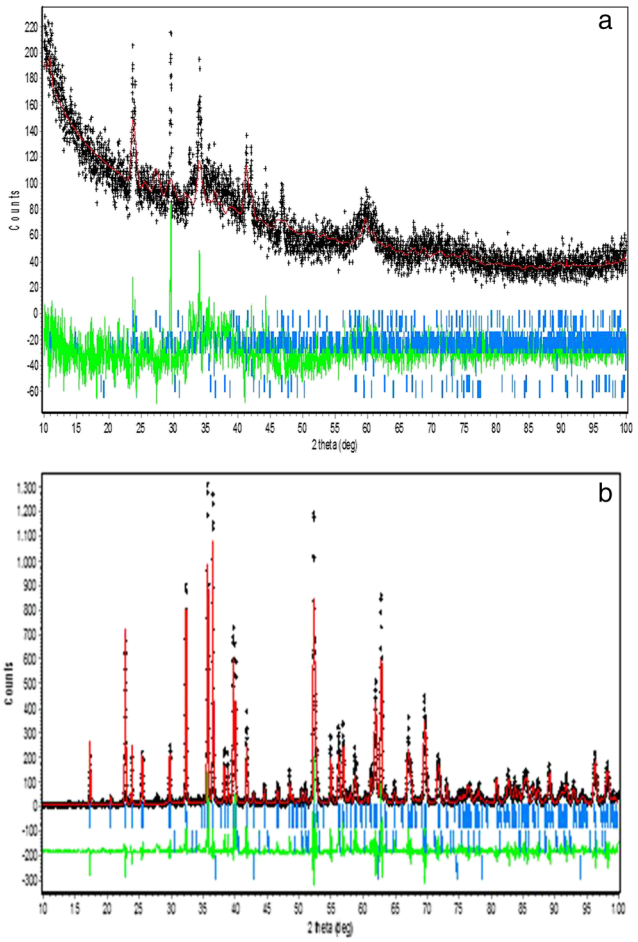

Fig. 3 XRD Rietveld plot for the sample non sintering (**a**) sintering at temperature 1300 °C (**b**). The observed data are shown by the plus sign and the calculated data by a solid line

increase in peak intensity of cristobalite and periclase may be attributed to their reaction to form forsterite through inter-diffusion between cristobalite and periclase took place, as has also been observed by others [39]. Further treatment of the sample at 1200 and 1300 °C was found to lead to increased amounts of forsterite, which suggest that higher temperatures have promoted the conversion of cristobalite and periclase into forsterite (Table 1). The cristobalite is most likely formed as a result of rice husk silica crystallization during the thermal treatment, while the periclase originated from magnesium. To verify the XRD results above, Rietveld analysis was used to obtain quantitative information on the phase composition of the samples. As representatives, the refined XRD patterns of the samples unsintered and sintered at 1300 °C are shown in Fig. 3a, b.

The structural of the best fits and quantitative results calculated by the Rietveld method for all samples are depicted in Table 1. The parameters R_{wp}, R_{exp}, R_p and the goodness of fit (GoF) indicate the quality of the fitting values relatively low according to the basic principle of GoF [40]. Therefore, perfect agreements were observed between the measured and the calculated patterns. As shown in Table 1, the amount of forsterite increased as the temperature of sintering increased, suggesting that the phase crystallization was started by sintering temperature addition of 1000 °C to produce a high amount of forsterite, which implies that more periclase reacted

Table 1 Figure of merits (FOMS) and weight percentage (wt%) from refinement of XRD data from refinement of XRD Data for the samples sintered at different temperatures for 6 h. Estimated errors for the least significant digits are given in brackets. (p = forsterite, q = cristobalite r = enstatite, s = silica, m = periclace

Temp (°C)	R_{exp}	R_{wp}	R_p	GoF	p	q	r	s	m
0	10.92	12.70	9.57	1.35	–	–	84.8 [3]	12.9 [4]	2.3 [2]
1000	15.35	17.31	17.22	1.27	87.7 [3]	6.4 [4]	–	–	5.9 [4]
1100	16.25	17.89	13.63	1.21	87.9 [4]	6.3 [5]	–	–	4.8 [2]
1200	15.40	17.03	12.87	1.22	88.7 [3]	6.6 [2]	–	–	4.7 [3]
1300	15.69	15.86	12.04	1.02	90.0 [2]	6.3 [4]	–	–	3.7 [4]

with silica to form forsterite. When the temperature sintering is higher than this limit (1000 °C), the periclace tends to dissolve in the silicate chain to form a forsterite phase and consequently the amount of forsterite continues to increase as the sintering of temperature increases.

The surface morphologies of the samples with different sintering temperature were compiled in Fig. 4a–d, indicating the significant effect of different sintering temperature on the size and distribution of the particles on the surface. With reference to XRD results (Table 1), it is obvious that the samples with a sintering temperature of 1000 to 1300 °C are mainly dominated by forsterite. As shown in Fig. 4a, b, the surface morphologies of the samples are characterized by the existence of particles with smaller grain and relatively uniform sizes on the surface, compared to those observed for the other two samples (Fig. 4c, d). The surface of the samples prepared at temperatures (1000 and 1110 °C) is dominated by small grains composed of forsterite clusters and covered some large grains of cristobalite and periclase. This feature suggests that at 1000 and 1100 °C, the cristobalite and periclase phases continue to change and allowed the particles to rearrange, leading to initiation of the formation of forsterite. The formation forsterite can be seen more clearly by inspecting the SEM micrographs of the samples treated at the temperature range of 1200–1300 °C (Fig. 4c, d), which displays intensified agglomeration on the entire surface as the temperatures increased. This agglomeration led to the intensified formation of forsterite as indicated by the XRD results (Table 1). This agglomeration phenomenon demonstrated that at the temperature range of 1200–1300 °C, the cristobalite phase has melted and reacted with the periclase phase to form forsterite. As is seen in Fig. 4c, d, SEM micrographs of the samples display quite significant differences in terms of the existence of particles with different grain sizes and the particle distributions. These images show that the highest formation of forsterite phase, as supported by XRD results (Table 1). Increase in grain size of forsterite causes a decrease in porosity that is proportional to the increased sintering of temperature. Moreover, the microstructure of the samples was found to display grains with relatively uniform sizes with the glassy surface without evident grain boundaries. These surface characteristics suggested that at these temperatures, the cristobalite phase has been converted into liquefied silica which penetrated the periclase phase, thus promoting the formation of forsterite as the dominant phase, as verified by the XRD results (see Table 1). With the Rietveld calculation, it was found that the quantity of forsterite increased from 87.7 to 90.0 wt% as temperature increased from 1000 to1300 °C.

Physical characteristics of synthesized refractory forsterite precursors with different sintered temperatures

The physical properties of the sintered samples at different temperatures are shown in Figs. 5(a, b), 6(a, b), and 7.

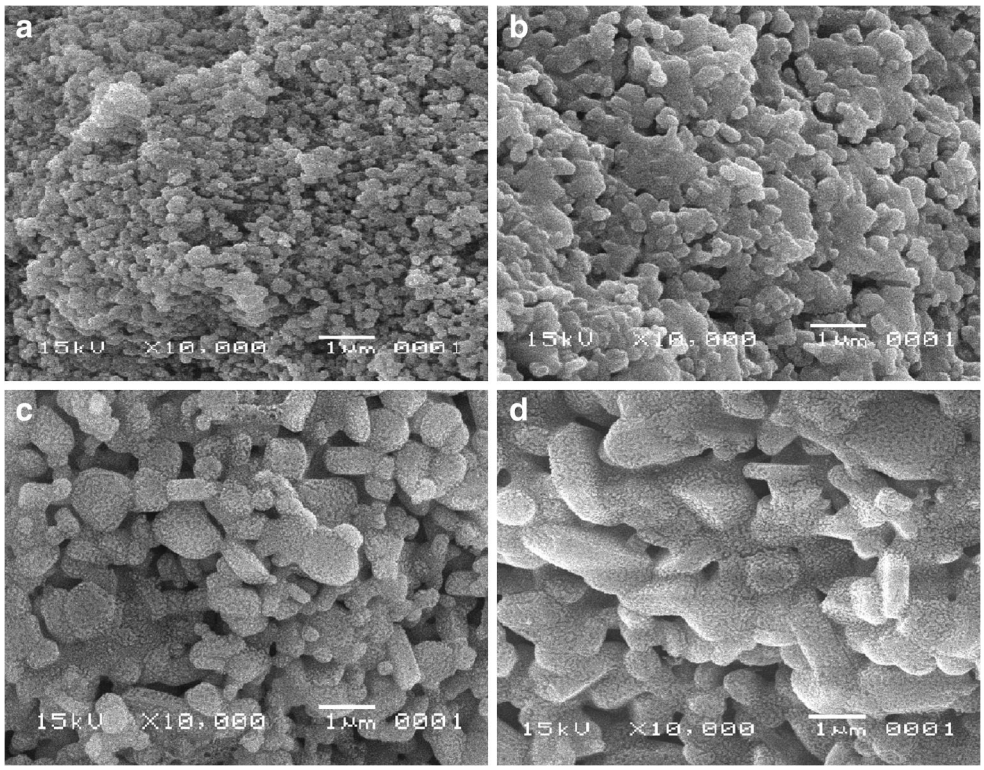

Fig. 4 The scanning electron microscopy (SEM) images of the samples sintered at different temperatures. **a** 1000 °C. **b** 1100 °C. **c** 1200 °C. **d** 1300 °C

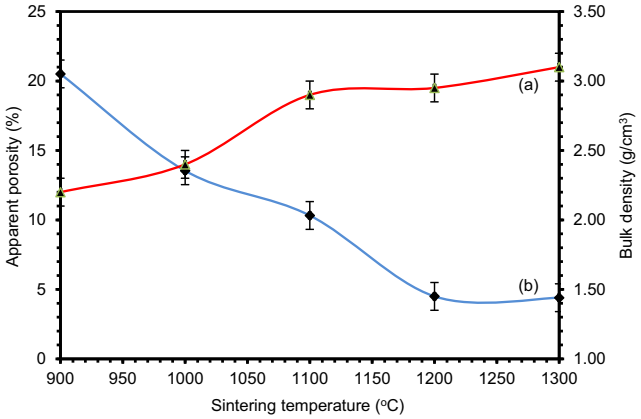

Fig. 5 Density (a) and porosity (b) as a function of sintering temperatures

Figure 5(a, b) shows the changes in density and porosity of the samples as a function of sintering temperatures.

As can be observed in Fig. 5(a, b), the density of the sintered samples increase sharply up to 1100, while the porosity of the sintered samples decrease sharply as the sintering temperatures increase up to 1200 °C, and beyond this temperature, relatively plat lines of the two characteristics were observed up to 1300 °C sintering temperature. As shown in Fig. 5(a), the densities of the sintered samples increase from 2.2 to 2.9 g/cm^3 as the sintering temperature increased from 900 to 1100 °C. The density was slightly increased and reached the value of 3.1 g/cm^3 at the sintering temperature of 1300 °C. The sharp increase of the density with increasing temperature up to 1100 °C, followed by a slow increase of the density with increasing temperature from 1100 to 1300 °C, was attributed to the increased amount of forsterite phase. The change in density was most likely due to reacting of periclase and silica into forsterite, as displayed by the XRD results presented in Table 1. These results are in accordance with the results of others [6], in which it was reported that the density of forsterite is 3.22 g/cm^3.

The sharp decrease of porosity with increasing temperature up to 1200 °C was attributed to the increased formation of forsterite phase, leading to decreased porosity. Beyond this

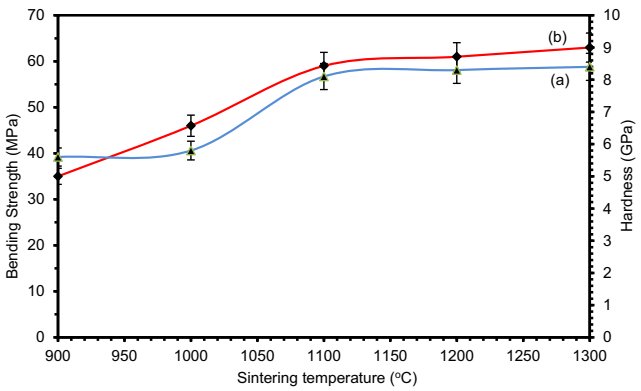

Fig. 6 Hardness (a) and bending strength (b) as a function of sintering temperature

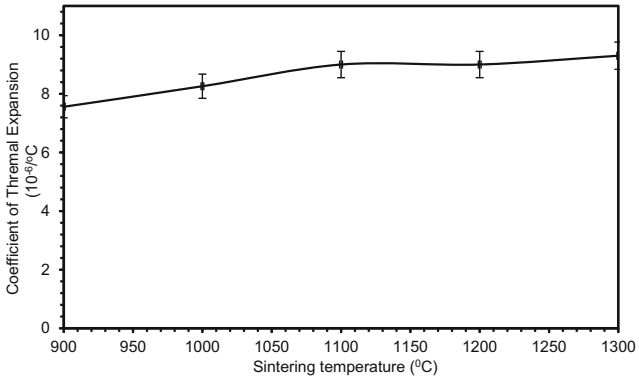

Fig. 7 Coefficient of thermal expansion of the sintered samples at different temperatures

temperature, porosity is slowly decreased, probably indicating the domination of forsterite, narrower particles distances, and also smaller pore in the samples as a result of higher sintering temperature applied, which is in accordance with the surface morphologies of the samples as seen in SEM results (Fig. 4c, d. Moreover, the porosity was found to decrease as the sintering temperature increased (Fig. 5(b)), which is in agreement with the increase in the amount of forsterite (see Table 1). These findings implied that at the temperature of 1300 °C, the sample has reached the vitrification point and transformed in the glassy state, leading to suppression of porosity.

Figure 6 shows the change in hardness and bending strength of the sintered samples, indicating that both characteristics increased as sintering temperature increased. As shown in Fig. 6(a), the higher the sintering temperatures, the larger the hardness, which implies that the samples became more compact as a result of increased amount of forsterite (Table 1).

The bending strength is sharply increased from sintering temperature of 900 to 1100 °C and relatively stable up to 1300 °C, as indicated by the practically plat line. This profile suggests that the bending strength can be considered as fully associated with the forsterite phase. From the practical point of view, this finding demonstrates that the hardness and bending strength of the samples can be controlled by controlling the formation of the forsterite phase, which is very useful for adjusting the suitability of the material for specified applications, such as insulator and conducting element in refractory devices. Other factors that control the hardness and bending strength are probably both the homogeneity of forsterite and the arrangement of the particles as a result of higher sintering temperatures applied, which is in accordance with the surface morphology of the samples, as shown in Fig. 4c, d.

Figure 7 shows the change in the thermal expansion coefficient of the samples as a function of sintering temperature. The results reveal that the thermal expansion coefficient of the samples increased drastically as the sintering

temperatures increase from 900 to 1100 °C and continuously increased from 9.0×10^{-6} to 9.3×10^{-6}/°C when sintering temperatures increased from 1110 to 1300 °C. It can be summarized that, as the sintering temperature increased, the coefficient of thermal expansion increased, most probably due to the increased in the amount of forsterite, as supported by XRD results (see Table 1) and the porosity decreased as confirmed by results (see Fig. 5). The trend observed in this study concerning the thermal expansion coefficient is consistent with the relationship between the thermal expansion coefficient and the volume fraction of the sample as described in the previous studies [41]. These previous studies explained that the thermal expansion coefficient was proportional to the volume fraction of materials in the composite and inversed with the porosity. It can be seen that coefficient of the thermal expansion of forsterite is higher than those of cristobalite, enstatite, and periclase, which are in agreement with the results described in the previous study [40]. More specifically, it was reported that the coefficient of thermal expansion of forsterite is 9.2×10^{-6}/°C [2] and cristobalite is 2.6×10^{-6}/°C [42], and the thermal expansion coefficient of enstatite is 7.9×10^{-6}/°C [43] and periclase is 8.0×10^{-6}/°C [44]. In accordance with the above values reported by others, it is then clear that increased the thermal expansion coefficient of the sample investigated in this study is most likely associated with the increased amount of forsterite (see Table 1), as a consequence of elevated sintering temperatures.

Conclusions

This work demonstrated that it is feasible to produce forsterite using rice husk silica with a heat treatment process. Heat treatment of the synthesized powder played pronounced effect on the formation of crystalline forsterite. Forsterite are formed from 1000 to 1300 °C, due to the reaction between silica from rice and periclace. FTIR results showed the presence of Si–O–Si, Si–O–Mg and Mg–O functional groups, which were associated with forsterite, cristobalite, and periclace as verified by XRD analysis. From Rietveld calculation, the forsterite formation started at 1000 °C and continued to grow at higher temperatures, resulting in increased weight percentage (wt%) from 87.7 to 90.0%, implying better forsterite crystal structure. The increasing of forsterite resulted in decreased porosity and increased in density, hardness, bending strength, and thermal expansion. Dense sintered samples with remarkably high hardness of 9.17 Gpa were achieved by sintering the sample at 1300 °C. Based on the physical characteristics of the prepared samples, this refractory can be envisaged as a thermal insulator, suggesting the potential use of the forsterite as refractory applications.

Funding information This work received research funding from the Ministry of Research, Technology, and High Education, Directorate General of Strengthening Research and Development, Republic of Indonesia provided through the Fundamental Research Grant Program, Batch II, 2018, with contract number: 062/SP2H/LT/DRPM/II/2018 and 384/UN26.21/PN/2018.

References

1. Deer, W.A., Howie, R.A., Zussman, J.: An Introduction to the Rock-Forming Minerals, 2nd edn. Pearson, London (1992)
2. Ye, Y., Schwering, R.A., Smyth, J.R.: Effects of hydration on thermal expansion of forsterite, wadsleyite, and ringwoodite at ambient pressure. Am. Mineral. **94**(7), 899–904 (2009)
3. Saberi, A., Alinejad, B., Negahdari, Z., Kazemi, F., Almasi, A.: A novel method to low temperature synthesis of nanocrystalline forsterite. Mater. Res. Bull. **42**(4), 666–673 (2007)
4. Diesperova, M., Bron, V.A., Perepelitsyn, V.A., Boriskova, T.L., Alekseeva, V.A., and Kelareva, E.I.: Forsterite refractories from the dunites of the kytlym deposits. Refrac. Indus. Ceram.18, 278–282 (1997)
5. Mitchell, M.B.D., Jackson, D., James, P.F.: Preparation and characterization of forsterite (Mg_2SiO_4) xerogels. Sol Gel Sci Technol. **13**, 359–364 (1998)
6. Ghomi, H., Jaberzadeh, M., Fathi, M.H.: Novel fabrication of forsterite scaffold with improved mechanical properties. Alloys Compd. **509**(5), L63–L68 (2011)
7. Tavangarian, F., Emadi, R.: Mechanical activation assisted synthesis of pure nanocrystalline forsterite powder. Alloys Compd. **485**, 648–652 (2009)
8. Martin, M.H.E., Ober, C.K., Hubbard, C.R., Porter, W.D., Cavin, O.B.: Poly(methacrylate) precursors to forsterite. Am Ceram Soc. **75**, 1831–1838 (1992)
9. Ni, S., Chou, L., Chiang, J.: Preparation and characterization of forsterite (Mg_2SiO_4) bioceramics. Ceram. Int. **33**, 83–88 (2007)
10. Fathi, M.H., Kharaziha, M.: Two-step sintering of dense, nanostructural forsterite. Mater. Lett. **63**(17), 1455–1458 (2009)
11. Mustafa, E., Khalil, N., Gamal, A.: Sintering and microstructure of spinel-forsterite bodies. Ceram. Int. **28**, 663–667 (2002)
12. Sasikala, T.S., Suma, M.N., Mohanan, P., Pavithran, C., Sebastian, M.T.: Forsterite-based ceramic-glass composites for substrate applications in microwave and millimeter wave communications. Alloys Compd. **461**, 555–559 (2008)
13. Amista, P., Cesari, M., Montenero, A., Gnappi, G., Lan, L.: Crystallization behaviour in the system $MgO\text{-}Al_2O_3\text{-}SiO_2$. Non-Crystal Solids 192&193, 529–533 (1992)
14. Hu, Y., Tsai, H.T.: Compositional effect on the crystallization of the cordierite-type glasses. Mater. Sci. **36**, 123–129 (2001)
15. Lacerda, S.R., Oliveira, J.M., Correia, R.N., Fernandes, M.H.V.: TiO-induced phase separation and crystallization in SiO_2-$3Ca{\cdot}P_2O_5$-MgO glass. Non-Crystal Solids. **221**, 55–60 (1997)
16. Khater, G.: Crystallizing phases from multi-component silicate glasses in the system $K_2O\text{-}CaO\text{-}MgO\text{-}Al_2O_3\text{–}SiO_2$. Ceram. Int. **27**, 661–668 (2011)
17. Demirci, Y., Günay, E.: Crystallization behavior and properties of cordierite glass-ceramics with added boron oxide. Ceram Proc Res. **12**, 352–356 (2001)
18. Lee, K.Y.S., Chin, K.M.C., Ramesh, S., Tan, C.Y., Teng, W.D., Sopyan, I.: Characterization of forsterite bioceramics. Adv. Mater. Res. **576**, 195–198 (2012)

19. Lee, Y.S.K., Chin, K.M.C., Ramesha, S., Purbolaksonoa, J., Hassana, M.A., Hamdia, M., Teng, T.D.: Characterization of forsterite ceramics. Ceram. Proc.Res. **14**(1), 131–133 (2013)
20. Haslinawati, M.M., Matori, K.A., Wahab, Z.A., Sidek, H.A.A., Zainal, A.T.: Effect of temperature on ceramic from rice husk ash. Int Basic Appl Sci. **09**(09), 22–25 (2009)
21. Rafiee, E., Shahebrahimi, S., Feyzi, M., Shaterzadeh, M.: Optimization of synthesis and characterization of nanosilica produced from rice husk (a common waste material). Int Nano Lett. **2**(29), 1–8 (2012)
22. Ugheoke, B.I., Mamat, O.: A novel method for high volume production of nano silica from rice husk: process development and product characteristics. Mater Engg Innov. **3**(2), 139–155 (2012)
23. Amutha, K., Ravibaskar, R., Sivakumar, G.: Extraction, synthesis and characterization of nanosilica from rice husk ash. Nano Technol Appl. **4**(1), 61–66 (2011)
24. Liou, T.H., Yang, C.C.: Synthesis and surface characteristics of nanosilica produced from alkali-extracted rice husk ash. Mater. Sci. Eng. B. **176**, 521–529 (2011)
25. Kordatos, K., Gavela, S., Ntziouni, A., Pistiolas, K.N., Kyritsi, A., Kasselouri-Rigopoulou, V.: Synthesis of highly siliceous ZSM-5 zeolite using silica from rice husk ash. Microporous Mesoporous Mater. **115**(1–2), 189–196 (2008)
26. Nayak, J.P., Bera, J.: Preparation of silica aerogel by ambient pressure drying process using rice husk ash as raw material. Trans Indus Ceram Soc. **68**(1–4), (2009)
27. Nayak, J.P., Kumar, S., Bera, J.: Sol-gel synthesis of bioglass-ceramics using rice husk ash as a source for silica and its characterization. Non-Crystal Solids. **356**, 1447–1451 (2010)
28. Watari, T., Nakata, A., Kiba, Y., Torikai, T., Yada, M.: Fabrication of porous SiO_2/C composite from rice husks. Eur CeramSoc. **26**, 797–801 (2006)
29. Martín, M.I., Andreola, F., Barbieri, L., Bondioli, F., Lancellotti, I., Rincón, J.M., Romero, M.: Crystallisation and microstructure of nepheline-forsterite glass-ceramics. Ceram. Int. **39**, 2955–2966 (2013)
30. Ngun, B.K., Mohamad, H., Sakai, E., Ahmad, Z.A.: Effect of rice husk ash and silica fume in ternary system on the properties of blended cement paste and concrete. Ceram. Proc. Res. **11**, 311–315 (2010)
31. Naskar, M.K., Chatterjee, M.: A novel process for the synthesis of cordierite ($Mg_2Al_4Si_5O_{18}$) powders from rice husk ash and other sources of silica and their comparative study. Eur Ceram Soc 2004; 24, 3499–3508 (2004)
32. Hossain, S.K.S., Mathur, L., Singh, P., Majhi, M.R.: Preparation of forsterite refractory using highly abundant amorphous rice husk silica for thermal insulation. JasCerS. **5**, 82–87 (2017)
33. Sembiring, S., Riyanto, A., Simanjuntak, W., and Situmeang, R.: Effect of MgO-SiO_2 ratio on the forsterite (Mg_2SiO_4) precursors characteristics derived from amorphous rice husk silica. Orient Chem 33 [4], 186–192 (2017)
34. Australian Standard. Refractories and refractory material physical test methods: the determination of density, porosity and water adsorption. 1–4, 1774 (1989)
35. Adam, F., Chua, J.H.: The adsorption of palmitic acid on rice husk ash chemically modified with Al(III) ion using the sol–gel technique. Coll Interf Sci. **280**(1), 55–61 (2004)
36. Kharaziha, M., Fathi, M.M.: Synthesis and charaterisation of bioactive forsterite nanopowder. Ceram. Int. **35**, 2449–2454 (2009)
37. Powder Diffraction File (Type PDF-2): Diffraction Data for XRD Identification. International Centre for Diffraction Data, PA, USA (1997)
38. Tavangarian, F., Emadi, R., Shafyei, A.: Influence of mechanical activation and thermal treatment time on nanoparticle forsterite formation mechanism. Powder Technol. **198**(3), 412–416 (2010)
39. Rani, A.B., Annamalai, A.R., Majhi, M.R., Kumar, A.H.: Synthesis and characterization of forsterite refractory by doping with kaolin. Inter. ChemTech Res. CODEN(USA). **6**(2), 1390–1397 (2014)
40. Kisi, E.H.: Rietveld analysis of powder diffraction patterns. Mater.Forum. **18**, 135–153 (1994)
41. Ono, T., Matsumaru, K., Juarez-Ramirez, J., Leticia, M., Torres-Martinez, Ishizaki, K.: Development of porous material with high Young's modulus and low thermal expansion coefficient in SiC-vitrified bonding material-$LiAlSiO_4$ system. Mater Sci Forum. **620-622**, 715–718 (2009)
42. Charles, A.H.: Handbook of Ceramic Glasses and Diamonds. McGraw Hills, Company Inc, USA (2001)
43. Hamzawy, E.M.A., Abd El Rahim, S.H., Melegy, A.A.: Composite-like material from magnesite, fumed silica and glass cullet Middle East. Appl. Sci. **4**(3), 455–459 (2014)
44. Buchanan, R.C.: Ceramic Materials for Electronics, 3d edn. University of Cincinnati, Cincinnati (2004)